Assessment of Defects and Amorphous Structure Produced in Raffinose Pentahydrate upon Dehydration

SIMON BATES,[1] RON C. KELLY,[1] IGOR IVANISEVIC,[1] PAUL SCHIELDS,[1] GEORGE ZOGRAFI,[2] ANN W. NEWMAN[1]

[1]SSCI, Inc., West Lafayette, Indiana 47906

[2]School of Pharmacy, University of Wisconsin-Madison, Madison, WI 57305

Received 7 September 2006; revised 4 November 2006; accepted 7 November 2006

Published online in Wiley InterScience (www.interscience.wiley.com). DOI 10.1002/jps.20944

ABSTRACT: The progressive conversion of crystalline raffinose pentahydrate to its amorphous form by dehydration at 60°C, well below its melting temperature, was monitored by X-ray powder diffraction over a period of 72 h. The presence of defects within the crystal structure and any amorphous structure created was determined computationally by a total diffraction method where both coherent long-range crystalline order and incoherent short-range disorder components were modeled as a single system. The data were analyzed using Rietveld, pair distribution function (PDF), and Debye total diffraction methods. Throughout the dehydration process, when crystalline material was observed, the average long-range crystal structure remained isostructural with the original pentahydrate material. Although the space group symmetry remained unchanged by dehydration, the *c*-axis of the crystal unit cell exhibited an abrupt discontinuity after approximately 2 h of drying (loss of one to two water molecules). Analysis of diffuse X-ray scattering revealed an initial rapid build up of defects during the first 0.5 h with no evidence of any amorphous material. From 1–2 h of drying out to 8 h where the crystalline structure is last observed, the diffuse scattering has both amorphous and defect contributions. After 24 h of drying, there was no evidence of any crystalline material remaining. It is concluded that the removal of the first two waters from raffinose pentahydrate created defects, likely in the form of vacancies, that provided the thermodynamic driving force and disorder for subsequent conversion to the completely amorphous state. © 2007 Wiley-Liss, Inc. and the American Pharmacists Association J Pharm Sci 96:1418–1433, 2007

Keywords: amorphous; crystal defects; water in solids; X-ray diffractometry; hydrates/solvates; crystallinity; crystal structure; raffinose pentahydrate; dehydration; pair distribution function (PDF)

INTRODUCTION

It is generally recognized that highly crystalline forms of active pharmaceutical ingredients (APIs) are preferred in the drug development process because of their high level of purity and resistance to physical and chemical instabilities under ambient conditions.[1] Organic crystals are generally imperfect in the structure of the crystal lattice, containing various types of crystal defects.[2] These defects represent regions of higher disorder relative to the three-dimensional long-range order expected and, hence, introduce a higher level of energy to the solid.[3] Pharmaceutical interest in such defects arises from the

Ron C. Kelly's present address is Amgen, South San Francisco, CA 94080.

Correspondence to: Ann W. Newman (Telephone: 765-463-0112; Fax: 765-463-2497; E-mail: Ann.Newman@aptuit.com)

Journal of Pharmaceutical Sciences, Vol. 96, 1418–1433 (2007)

demonstrated role that these high energy sites can play in affecting a number of important physical and chemical phenomena, including higher dissolution rates,[4] greater chemical instability,[5,6] altered mechanical properties,[7–9] and enhanced hygroscopicity.[10,11] Such effects of disorder on solid-state properties of crystals also occur when the solid is converted fully or in part to the amorphous state, such that it has lost long-range order but has retained the short-range order observed with liquids.[12] The relationship between crystal defects and the amorphous form of solids can be thought of in terms of the extent of defect density in the solid and the increasing landscape of potential energy minima that arise with increasing density.[13] Thus the formation of amorphous regions occurs with the spatial coalescence of defects.[14] In this regard, therefore, it is not surprising that processes, such as milling and compaction, that can give rise to crystal defects, in the extreme case, eventually can give rise to completely amorphous materials with greatly enhanced changes in physical and chemical properties of the solid.

The issue that we wish to pursue in this study is the extent to which we might be able to quantitatively observe the formation of crystal defects during a pharmaceutical process that introduces disorder into the crystal, as well as to determine the subsequent coalescence of such defects into the amorphous state. To this end we report a study using X-ray powder diffraction (XRPD) data combined with Rietveld modeling and total scattering analysis for samples of raffinose pentahydrate subjected to increasing levels of dehydration, where the introduction of both defects and amorphous structure is followed quantitatively. The presence of random defects within a crystal structure will generate diffuse X-ray scattering much like X-ray amorphous scattering. As the defects represent random deviations from an average crystal structure, the form of the diffuse scattering will, in most cases, be markedly different than a true amorphous phase where the long-range order has collapsed. (This may not be true for a material that forms a kinetic glass.) The difference in the shape of the diffuse scattering profile allows some differentiation between defect and amorphous levels in a sample. In addition to the increased diffuse scatter, the presence of random defects will cause a drop in diffraction peak intensities at higher measurement angles, similar to an increased thermal Debye–Waller effect. This loss in high angle peak intensity should not be visible for mixed amorphous/crystalline systems.

Raffinose, the trisaccharide, β-D-fructofuranosyl-o-α-D galactopyranosyl-(1 → 6)-α-glucopyranoside, normally exists as the pentahydrate crystal with no known ability to exist as a stable unsolvated or anhydrous crystal.[15–17] In a previous study,[17] it was shown that when the pentahydrate is stored at 10% relative humidity (RH) and room temperature for a period of up to 3 months, it loses only one water molecule. An additional water molecule was lost within 24 h when it was stored at 30°C in a vacuum oven. In both cases the original crystal structure of the pentahydrate was retained, and both waters were rapidly restored by exposure to elevated RH. Increasing the temperature to 60°C and storing for over a period of 24–48 h progressively removed the remaining water molecules, causing the crystal to eventually collapse into an amorphous form having a glass transition temperature (T_g) and water sorption profile that was essentially identical to that of a sample prepared by lyophilization. Subsequent studies have confirmed the formation of amorphous raffinose by dehydration of the pentahydrate, and have further analyzed the amorphous material through measurements of molecular mobility, fragility, and recystallization tendencies.[18–20] Similar dehydration studies have been reported for trehalose dihydrate,[21–23] and it was found that the rate of dehydration influences the material produced. A slow dehydration promotes the formation of an anhydrous crystalline phase (α) of trehalose, whereas a fast dehydration promotes the formation of an amorphous phase.[21,22] In another study, removal of water resulted in an amorphous material and it was suggested that the progressive removal of water molecules should bring the crystal to a state of absolute mechanical instability in which spontaneous collapse to some other phase would be inevitable.[23] Then, vitrification occurs by nucleation and growth of the amorphous phase in an intriguing inversion of the familiar process of crystallization of metastable liquids.[23]

It is the intent of this study to evaluate by XRPD measurements the possibility that the initial loss of water from raffinose pentahydrate (the first few water molecules), caused by application of thermal energy, produces vacancies and other defects that upon further dehydration coalesce to produce increasing levels of amorphous raffinose.

EXPERIMENTAL

Materials

D-(+)-raffinose pentahydrate (lot no. 075K0018) was obtained from Sigma Chemical Company (St. Louis, MO) and used as received.

Methods

Dehydration

Amorphous and defected raffinose samples were prepared by dehydration. Approximately 200 mg of D-(+)-raffinose pentahydrate was placed into separate glass scintillation vials. The vials were placed uncapped into a 60°C vacuum oven. Samples were removed at predetermined time intervals (0.5, 1, 2, 5, 8, 24, 48, and 72 h). The samples were stored in a desiccator until ready for analysis. Solid form identification was confirmed by XRPD.

X-ray Powder Diffraction

XRPD analyses were performed using an Inel XRG-3000 diffractometer (Stratham, NH) equipped with a curved position sensitive (CPS) detector with a 2θ range of 120°. Real time data were collected using Cu Kα radiation starting at approximately 4°2θ at a resolution of 0.03°2θ. The tube voltage and amperage were set to 40 kV and 30 mA, respectively. The pattern is displayed from 2.5 to 60°2θ. Samples were prepared for analysis by packing them into thin-walled glass capillaries. Each capillary was mounted onto a goniometer head that is motorized to permit spinning of the capillary during data acquisition. The samples were analyzed for approximately 60 min at ambient temperature. Instrument calibration was performed using a silicon reference standard.

Due to uncertainty introduced into the analysis of the diffuse X-ray amorphous scattering by variations in the glass capillary background, XRPD analyses for the amorphous samples were performed using a Shimadzu XRD-6000 X-ray powder diffractometer (Kyoto, Japan) using Cu Kα radiation. The Bragg–Brentano reflection geometry gives a lower background signal that is easier to model and remove from the diffuse X-ray amorphous contribution. The Shimadzu instrument is equipped with a long fine focus X-ray tube. The tube voltage and amperage were set to 40 kV and 40 mA, respectively. The divergence and scattering slits were set at 1° and the receiving slit was set at 0.15 mm. Diffracted radiation was detected by a NaI scintillation detector. A θ–2θ continuous scan at 1.2°/min from 2.5 to 60°2θ was used with an effective 0.04 step size. The analysis was performed at ambient temperature. A silicon standard was analyzed to check the instrument alignment. Data were collected and analyzed using XRD-6100/7000 v. 5.0. Samples were prepared for analysis by placing them in an aluminum sample holder with silicon inserts. During the analysis, the samples were spun at 30 rpm. Although the diffuse X-ray amorphous contribution is more accessible from the Bragg–Brentano measurements, there was significant variability in the crystalline diffraction, most likely due to large crystal size and preferred orientation. The original Inel data were used for analysis of the crystalline material and the Shimadzu data were used for analysis of the diffuse scattering.

Karl Fischer

Coulometric Karl Fischer (KF) analysis for water determination was performed using a Mettler Toledo DL39 Karl Fischer titrator (Columbus, OH). Approximately 30 mg of sample was placed in the KF titration vessel containing approximately 120 mL of Hydranal–Coulomat AD and mixed for 60 s to ensure dissolution. Three replicates were obtained to ensure reproducibility.

Differential Scanning Calorimetry

Differential scanning calorimetry (DSC) was performed using a TA Instruments differential scanning calorimeter 2920 (New Castle, DE). The sample was placed into an aluminum DSC pan, and the weight accurately recorded. The pan was covered with a lid without crimping. For studies of the T_g of the amorphous material, the sample cell was equilibrated at 25°C, then heated under nitrogen at a rate of 20°C/min, up to 150°C. The sample cell was then allowed to cool and equilibrate at −20°C. It was again heated at a rate of 20°C/min up to 150°C, and then cooled and equilibrated at −20°C. The sample cell was then heated at 20°C/min up to a final temperature of 200°C. The T_g is reported as the onset of the

 DOI 10.1002/jps

transition. Indium metal was used as the calibration standard.

Computational Studies

The analysis of defects within a crystalline structure requires a total diffraction methodology where both the coherent long-range crystalline contributions and incoherent short-range disorder components are modeled together as a single system.[24,25] However, to take advantage of traditional Rietveld methods for structure modeling and to better present the diffuse scattering, analysis of the two contributions will be presented separately in this paper. The measured data were passed through a series of digital band pass filters to isolate the crystalline diffraction peaks from the diffuse scattering halo and in the process remove the instrumental background. For the transmission capillary measurements, the digital filter band pass was set to isolate the crystalline diffraction peaks for Rietveld analysis, removing the majority of the diffuse and background components. The diffuse scattering was isolated from the reflection measurements, requiring a reasonable estimation of the instrumental background. The initial modeling pass treated the instrumental background as being linear with a primary beam spill over and an air scatter term modeled as a combination of Lorentzian plus Lorentzian squared contributions. The band pass filter was carefully tuned to closely follow the base of the diffraction peaks while still maintaining a smooth curve. The diffuse component extracted from the as-received sample before drying will contain the higher order background terms including Compton scattering and thermal diffuse scattering in addition to any equilibrium defect scattering. The diffuse component from the as-received material was used as an estimate of the higher order background terms and was removed from the diffuse scattering of the dehydrated samples after scaling for the sample mass and crystalline content. The residual diffuse components for the dehydrated material were analyzed using a total scattering approach to model the local disorder induced by the drying process.

Rietveld Method

The Rietveld method was originally developed for single crystal structure solution,[26,27] and provides a powerful tool for tracking structural phase changes in crystalline material. Although the Rietveld method works well for crystalline material the applicability of the method begins to fail for more disordered systems.[28] Defect scattering is not modeled in the traditional Rietveld methods and must be treated separately. The Rietveld analysis results presented here were derived using MAUD, v.2.043.[29]

The Rietveld method was applied to crystalline diffraction measured on the Inel instrument in order to track the structural changes taking place during the dehydration process. The initial crystalline model was taken from the published single crystal structure of raffinose pentahydrate in the Cambridge Structural Database[30] (Ref codes RAFINO[15] and RAFINO01[16]). The increasing diffuse background was modeled as a seventh-order polynomial with two Gaussian components. The change in molecular packing between the pentahydrate and trihydrate was modeled using rigid versions of the molecules as described in the pentahydrate crystal structure. The water molecules and rigid raffinose molecules were allowed to freely move and rotate without any constraining force fields or hydrogen bonding requirements. Although a harmonic fiber preferred orientation model was required to correctly describe the measured intensities for the pentahydrate data, no preferred orientation was required to model the lower hydrate data. In addition to the rigid molecule refinement and background, the unit cell parameters (a, b, c) and crystal size were allowed to vary during the Rietveld modeling.

Pair Distribution Functions (PDF)

One of the most generally useful tools for total diffraction analysis is the PDF. The PDF provides a fingerprint of the interatomic distances that define a particular solid form[31] and is very useful for determining relationships between ordered and disordered systems. The PDF is generally presented as probability against distance and represents the weighted probability of finding two atoms separated by a distance r.[32] The peaks in the PDF correspond to commonly occurring interatomic distances, where the product of peak area and distance gives the number of atom units with that specific pair separation. A PDF trace is a robust one-dimensional representation of a radially averaged three-dimensional structure,[33–37] as shown in Figure 1b. Additional information on PDF can be found elsewhere.[28,38–41] PDF analyses performed in this

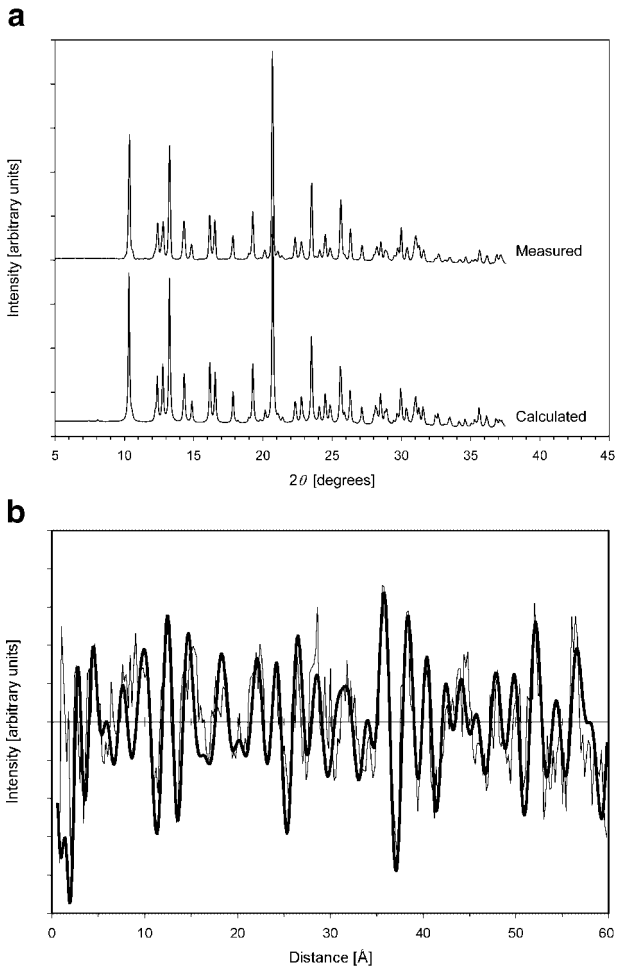

Figure 1. (a) XRPD patterns for raffinose pentahydrate measured for the as received (bold line) and calculated by Rietveld refinement of the single crystal structure (thin line), (b) PDF derived from the crystalline component of the measured XRPD pattern for the as-received material (bold line) and from the calculated XRPD pattern (thin line). Rietveld refinement performed using single crystal structure of raffinose pentahydrate (REFCODE: RAFINO01).

study used software developed internally based on published equations.[38]

In this study the PDF method was applied to the crystalline component of the diffraction pattern, as extracted by the digital filter, in order to confirm the structural changes proposed by the Rietveld modeling. A theoretical PDF can be calculated from the structural solution proposed by the Rietveld modeling which can then be compared with the experimentally derived PDF to verify the consistency of the Rietveld structure solution.

The PDF, *G(r)* is calculated from a known single crystal structure using the relationships defined in Eq. 1 and 2.

$$G(r) = 4\pi r[\rho(r) - \rho_0] \tag{1}$$

where ρ_0 is the average number density of the structure and $\rho(r)$ the atom pair density for X-ray scattering is given by Peterson:[42]

$$\rho(r) = \left(\frac{1}{4}\pi r^2\right) \sum_{p,q} \left(\frac{f_p f_q}{\langle f \rangle^2}\right) \delta(r - r_{pq}) \tag{2}$$

where $f_{p,q}$ is the individual atomic form factors and $\langle f \rangle$ represents a mean atomic form factor for the structure. The distance r_{pq} represents the atom pair separation and $\rho(r)$ represents the probability of finding an atom pair separated by the distance "r" weighted by the atomic form factors and averaged over all pairs in the structure. The pair sum must be performed over a crystal structure large enough to give the full atom pair relationships out to the distance of interest.

Defect Scattering

The presence of random defects within a crystal structure will generate diffuse X-ray scattering much like X-ray amorphous scattering in appearance. Many of the general approaches to percent crystallinity determination using X-ray methods will include the scattering from defects as an amorphous contribution. In this work, the diffuse scattering from defects was isolated from the X-ray amorphous scattering to provide a more robust model of the dehydration process.

The lack of distinctive features in diffuse X-ray scattering from disordered systems can lead to any number of different conclusions as to the origin and nature of the diffraction. One of the recognized methodologies in dealing with this inherent ambiguity[21] is to start with realistic molecular models of the disorder and then back calculate the corresponding diffuse scattering profile. The simplest random defect model for the diffuse profile can be derived from the Debye–Einstein approach to thermal scattering as outlined in Cowley[2] (Eq. 3). This model has one variable parameter, the root mean square (RMS) lattice distortion (Δ) in Å corresponding to the mean lattice distortion established by the defects. The application of the Debye–Einstein

 DOI 10.1002/jps

approach requires the derivation of the continuous unit cell structure factor *F(Q)*, which can be derived using the Debye sum presented in Eq. 4. The implicit assumption of this simple model is that the defects occur randomly as single noninteracting events.

$$I_D(Q) = I_0 PF(Q)(1 - \exp(-Q^2\Delta^2/2)) \quad (3)$$

I_0 is a simple scale factor and P represents the standard polarization correction $(1+\cos(2\theta)^2)/2$ for laboratory X-ray diffraction measurements without a monochromator.

$$F(Q) = \sum_p (f_p^2) + 2^* \sum \sum (f_p f_q \sin(Q\underline{r}_{pq})/(Q\underline{r}_{pq})) \quad (4)$$

The first sum over the square of the individual atomic form factors f_p represents the self-scattering contribution. The double sum is evaluated over each atom pair *(p,q)* in the symmetric unit cell where r_{pq} is the atom pair separation distance. The use of the Debye sum to evaluate the continuous structure factor assumes a random orientation of unit cells within the sample. A solid-state matrix correction must be applied to the Debye calculation in Eq. 4 to remove the spurious small angle scattering signal arising from the small unit cell size.[43]

The diffuse scattering profiles extracted using the digital filter from the measured data were modeled using the Debye–Einstein approach as expressed in Eq. 3 to determine if a random noninteracting defect model is an appropriate description of the initial dehydration process for raffinose.

Crystalline to Amorphous Conversion

If the conversion from crystalline material to amorphous is assumed to be a random and noncooperative process, then it is straightforward to derive a functional form for the expected amorphous percentage after different drying times, as shown in Eq. 5.

$$\text{Amorphous } \% = C_R\{\exp(-0.1\delta t) \times (\exp(0.1(\delta t + 1)) - 1)/ (\exp(0.1) - 1) - 1\} \quad (5)$$

where C_R is the interconversion rate (percent/hour) and δt is the time in hours. This equation is exact for slow conversion rates less than 0.1% per hour, and provides a good approximation for faster conversion rates.

RESULTS AND DISCUSSION

Raffinose Pentahydrate

The single crystal structure of raffinose pentahydrate[15,16] shows two distinct locations for the water molecules. Three water molecules act as both hydrogen bond donors and acceptors in a complex hydrogen bond network with raffinose. The other two water molecules act only as hydrogen bond donors (one to raffinose and one to water) and exhibit longer and weaker bonding than the other three water molecules. Based on these observations, it is likely that the latter two waters would initially leave the structure upon dehydration, as previously suggested.[17]

KF data collected on the sample established that the material contained five moles of water. The experimental XRPD pattern of the raffinose pentahydrate starting material was well described using the Rietveld method based upon the single crystal structure in the Cambridge Structural Database[27] (Ref code RAFINO01[16]), confirming that the material received from Sigma is raffinose pentahydrate (Fig. 1a). A small harmonic preferred orientation correction was required to achieve the best fit to the measured intensities. The crystal unit cell required minor expansion in volume from the RAFINO01[16] unit cell, bringing it close to the RAFINO[15] structure in the CSD, as summarized in Table 2. In Figure 1b, the PDF as calculated from the Rietveld pentahydrate crystal structure is compared with the PDF derived from the crystalline component of the Inel data on the as-received material. Although the calculated PDF does not have any corrections for preferred orientation, the overall agreement is good, not only confirming the pentahydrate structure but also demonstrating the self-consistency of the PDF calculation method.

Dehydration Studies

Raffinose pentahydrate was heat treated under vacuum to examine the material at various stages of dehydration and the data are summarized in Table 1. Slight changes in the crystalline powder patterns were evident during drying. After 24 h of drying the patterns show mainly an amorphous halo. The T_g of the amorphous material obtained after 24 h of drying was determined to be approximately 94°C, which is similar to values reported previously.[17] The

Table 1. Summary of Processed Raffinose Pentahydrate Samples

Time (h)[a]	XRPD Result
0	Crystalline
0.5	Crystalline
1	Crystalline + amorphous
2	Crystalline + amorphous
5	Crystalline + amorphous
8	Crystalline + amorphous
24	Mainly amorphous[b]
48	Amorphous
72	Amorphous

[a]Time in 60°C vacuum oven.
[b]Crystalline peaks present cannot be modeled by Rietveld.

dehydration conditions, and therefore the kinetics of the water removal, were similar to those reported previously.[17]

Changes in Crystalline Material

The Inel XRPD data for dehydrated raffinose pentahydrate exhibited crystalline diffraction peaks even after 8 h of heating, as shown in Figure 2. It is evident that the peak intensities appear to decrease and the background increases with longer heating times. Two relatively small diffraction peaks appeared at low angles upon dehydration that were not present in the starting pentahydrate powder pattern. These peaks are allowed reflections within the $P2_12_12_1$ space group of raffinose pentahydrate, so their appearance is not indicative of a significant rearrangement in the molecular packing motif, but they do indicate a structural change occurring upon dehydration.

Rietveld modeling of the XRPD data was performed to look at changes in the lattice parameters upon dehydration and to model the structural changes. The lattice parameters from the single crystal structure RAFINO[15] are also included for comparison with the as-received material. Good agreement was obtained between the single crystal structure values and the lattice parameters determined from the Rietveld analysis. The modeling results showed that the space group of the crystal structure ($P2_12_12_1$) remained unchanged upon drying; however, the lattice parameters for the treated samples were found to vary, as summarized in Table 2. As shown in Figure 3, both the reflection and transmission measurements show matching behavior for the *c*-lattice parameter, which initially remains relatively unchanged for the 0.5 and 1 h drying times. At the 2 h drying point there is a rapid decrease in the *c*-lattice parameter of up to 0.7%. By 5 h of drying, the *c*-lattice parameter decreases further giving a total change of approximately 1.3% from the original pentahydrate structure. After 8 h of drying the *c*-lattice parameter remains relatively unchanged from the 5 h drying value. These data indicate that after an initial change in crystal structure between 1 and 2 h of drying, the new lower hydrate structure remained relatively stable with continued heating. Looking at the

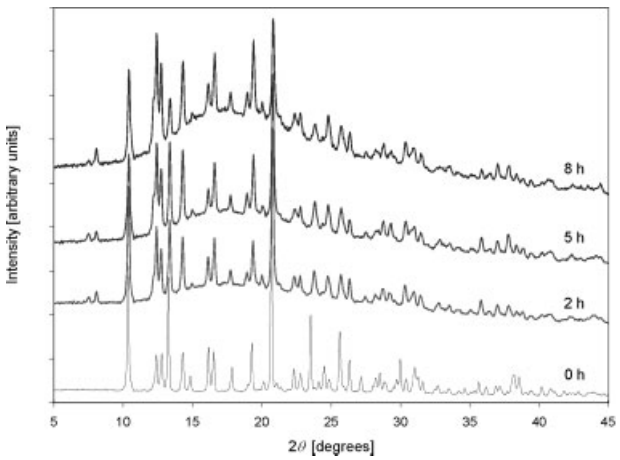

Figure 2. XRPD patterns (transmission) for raffinose pentahydrate dried at 60°C under vacuum for (from bottom to top): 0, 2, 5, and 8 h.

Table 2. Unit Cell Parameters of Raffinose Pentahydrate Samples

Time (h)[a]	*a* (Å)	*b* (Å)	*c* (Å)	Volume (Å^3)
RAFINO[b]	8.966	12.327	23.837	2634.6
0 (as received)	8.967	12.357	23.873	2645.3
2	9.015	12.433	23.618	2647.2
5	9.006	12.432	23.560	2637.8
8	9.011	12.420	23.551	2635.7
0 (as received)[c]	9.0318	12.341	23.872	2660.8
0.5[c]	9.028	12.366	23.867	2664.5
1[c]	8.991	12.369	23.905	2658.5
2[c]	9.063	12.384	23.778	2668.8
5[c]	9.137	12.428	23.562	2675.6
8[c]	9.135	12.417	23.556	2671.9

[a]Hours in 60°C vacuum oven.
[b]From reference 15.
[c]Derived from reflection measurements with lower accuracy.

 DOI 10.1002/jps

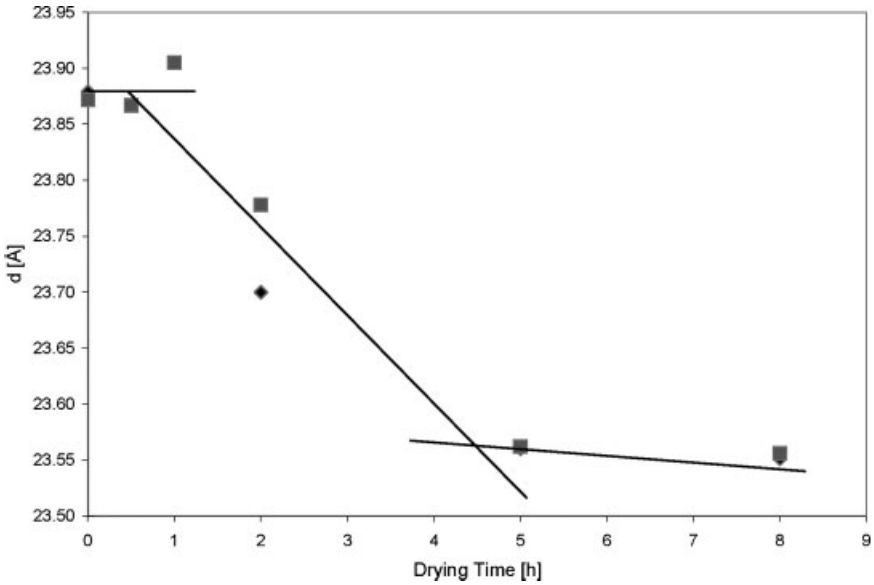

Figure 3. Change in the *c* lattice parameter of raffinose pentahydrate with drying time obtained from Shimadzu (reflection) (■) and Inel (transmission) (◆) diffractometers.

unit cell volume numbers in Table 2 for the transmission measurements, the overall decrease in the volume by 8 h is equivalent to the volume of a single water molecule. With two water molecules per raffinose being lost as reported previously,[17] there is only elastic recovery for a single water molecule. The remaining lost waters are proposed to create "vacancies" within the original pentahydrate structure.

The structures were also probed using PDF analysis. The PDF transform for samples after 2, 5, and 8 h of drying is shown in Figure 4a. A small loss of crystallinity was evident as a function of drying time based on the progressive damping of the PDF oscillations at larger distances. Aside from the crystallinity loss, the PDF patterns are very similar, supporting the conclusion from the Rietveld analysis that the raffinose crystal structure is stable between 2 and 8 h of drying. When the PDF of the initial pentahydrate material was compared to the sample dried for 2 h (Fig. 4b), there was significant peak shifting observed for a small subset of the PDF peaks. These data are in agreement with the lattice parameter calculations indicating the initial change in crystal structure before the 2 h drying point. The new lower hydrate crystal structure formed by the drying process is isostructural with the original pentahydrate. The space group remains unchanged and the majority of the original PDF peaks are unaffected by the transformation.

The XRPD data were used within a Rietveld refinement to determine the change in molecular packing that occurs during the initial 2 h of drying. The XRPD data alone may not be able to distinguish the hydration state; however, based upon analysis of the hydrogen bonding within the crystal structure, the new crystal form was modeled as a trihydrate. Water molecules 1 and 5 were intentionally removed from the pentahydrate structure before the trihydrate structure was modeled. These waters are not expected to be bound tightly within the structure since both are involved in two hydrogen bond interactions, where only one (serving as a H-bond donor) directly involves a raffinose molecule.[15,16] During modeling, the raffinose molecule was treated as being a rigid body with full rotation and translation degrees of freedom. The water molecules were allowed free movement independent of the raffinose molecule with no hydrogen bonding restrictions imposed. The unit cell obtained is given in Figure 5a. The trihydrate crystal form is orthorhombic with a $P2_12_12_1$ space group and unit cell parameters $a = 9.013$ Å, $b = 12.422$ Å, and $c = 23.556$ Å.

Although the spatial resolution achievable from the powder patterns used in this study is limited to approximately 2.5 Å and bearing in mind that the rigid molecule approximation may influence the location of individual water molecules, it is nevertheless instructive to investigate the

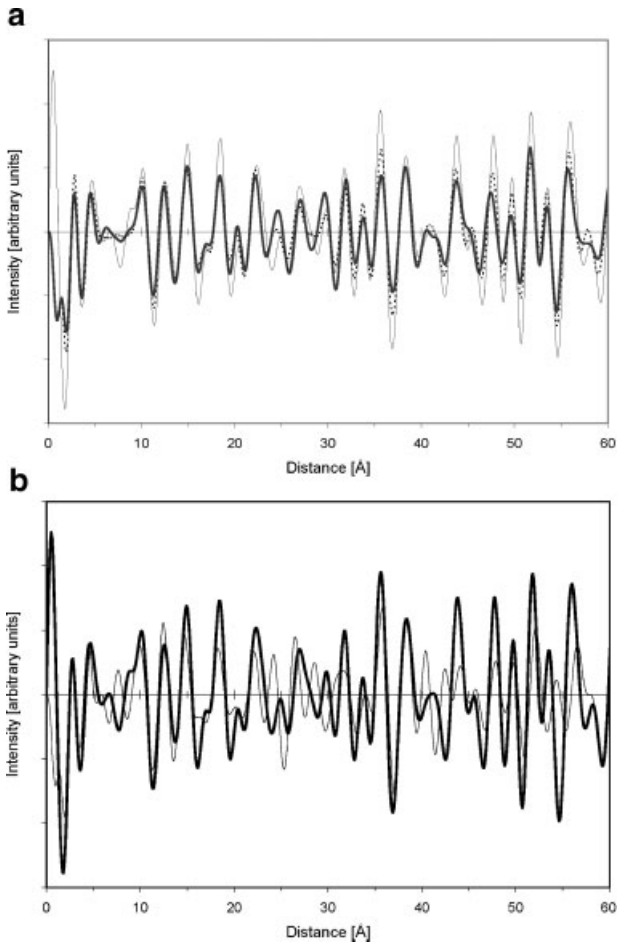

Figure 4. PDF of (a) samples dried for 2 h (thin line), 5 h (dashed line), and 8 h (bold line) and (b) raffinose pentahydrate as received (thin line) and the dried sample after 2 h (bold line).

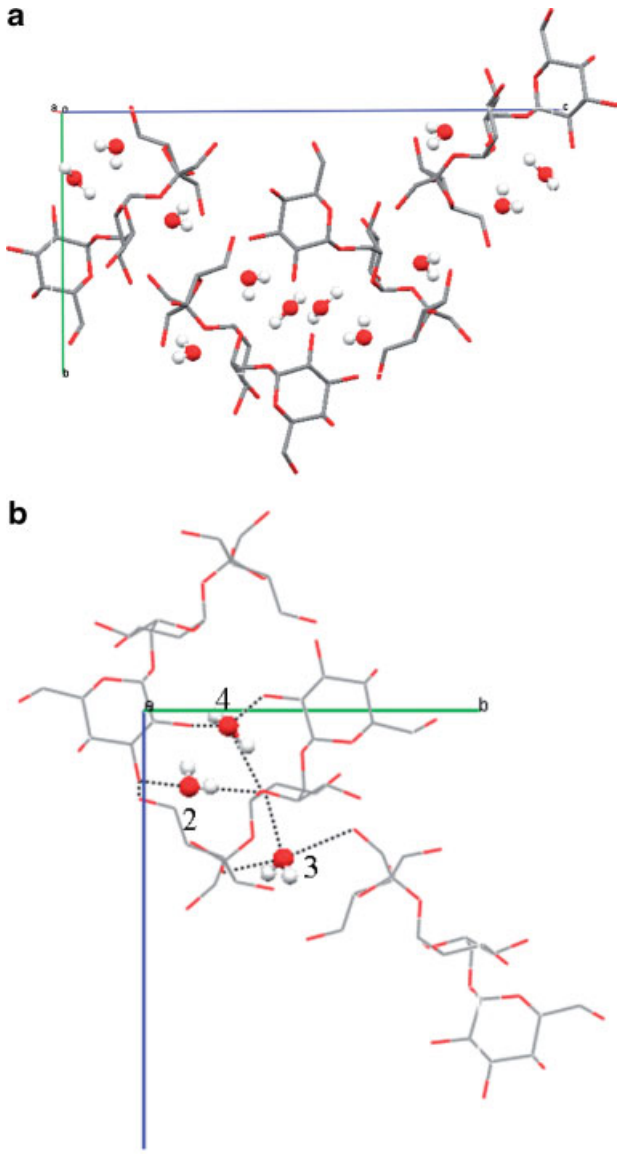

Figure 5. (a) Unit cell of raffinose trihydrate. (b) Hydrogen bonding of water molecules in raffinose trihydrate crystal structure.

resulting structure in terms of the hydrogen bonding. The structure of the pentahydrate is compared to the calculated trihydrate structure in Figure 6. The calculated trihydrate structure has two water molecules (2 and 4) per raffinose located in a channel. The other water molecule (water 3) is located outside of the channel (Figs. 5b and 6b). Similar to the pentahydrate, the hydrogen bonding between the water and raffinose molecules is extensive. It was previously reported that the water molecules in the pentahydrate crystal structure interact through both accepting and donating hydrogen bonds with each other and with raffinose.[15,16] The primary hydrogen bond interactions are maintained in the trihydrate structure with the exception of water 2. In the trihydrate structure, slight rotations of the raffinose molecules cause water 2 to accept and donate only one hydrogen bond to raffinose (Fig. 6b). In contrast, water 2 in the pentahydrate structure accepts and donates one hydrogen bond to raffinose and donates one hydrogen bond to water.[15,16]

Figure 7 shows the overlay of the PDF trace derived from the measured crystalline data from material exposed to 8 h of drying compared to the simulated PDF trace based upon the proposed raffinose trihydrate crystal structure. The overall correlation is similar to that observed for the known pentahydrate structure (Fig. 1b), although the slight mismatch in structure at approximately 6.8 Å reappears at the harmonic positions of

 DOI 10.1002/jps

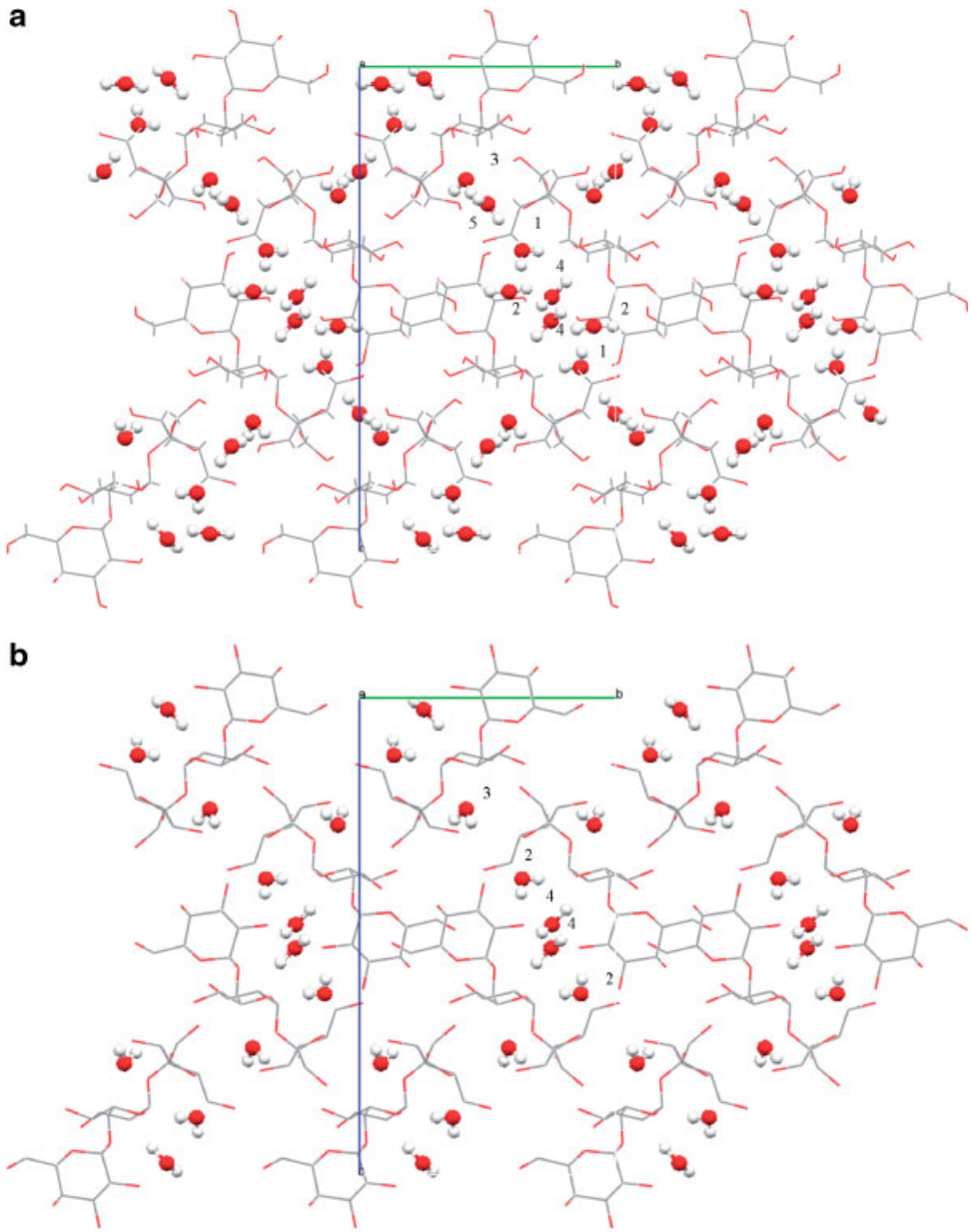

Figure 6. Crystal structure of raffinose pentahydrate (a) and calculated trihydrate structure (b) showing location of the water molecules.

approximately 27.2 and 40.8 Å. This may indicate a distortion in the proposed structure away from the true trihydrate crystal structure, which may arise from the rigid molecule approximation.

The analyses performed on the crystalline patterns indicate that the loss of water does not change the crystalline space group. The dehydration does, however, cause an observable change in the unit cell parameters with a corresponding unit cell volume change equivalent to a single water molecule. These seemingly minor changes in structure could ultimately change the properties of the solid, resulting in inconsistent material being produced.

Defects and Amorphous Regions

Dehydration beyond 8 h resulted in mainly amorphous patterns, as shown in Figure 8. The initial removal of water likely creates the initial defects in the crystalline material as observed by XRPD, which then results in X-ray amorphous

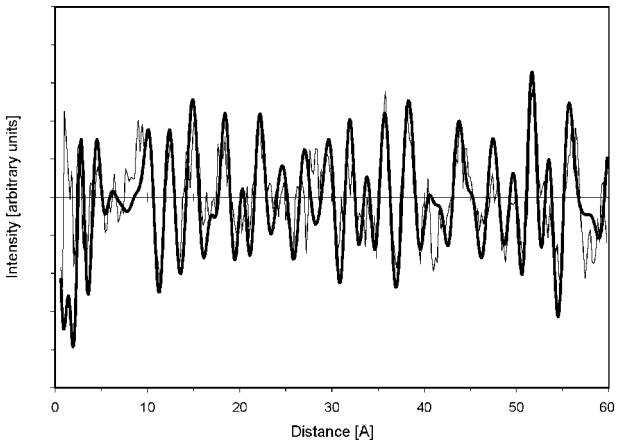

Figure 7. PDF of calculated trihydrate structure (thin line) and sample after drying at 60°C under vacuum for 8 h.

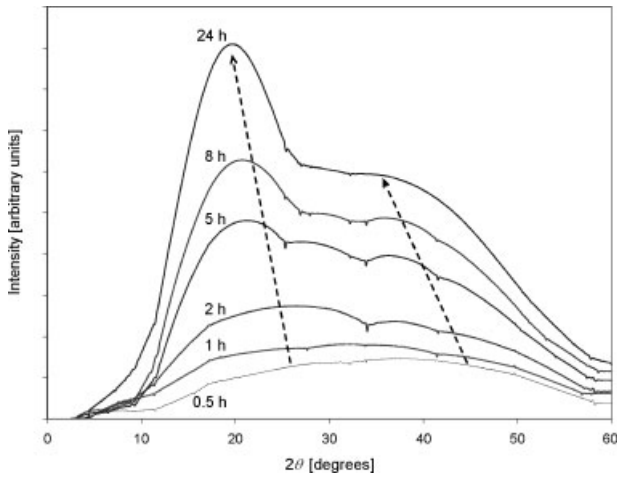

Figure 9. Diffuse scatter due to dehydration of raffinose pentahydrate at 60°C under vacuum for (from bottom to top): 0.5, 1, 2, 5, 8, and 24 h.

patterns upon full dehydration. In order to further understand the defected material, the diffuse scattering from the XRPD data was investigated.

The diffuse scattering data were obtained using a digital band pass filter on the XRPD data collected using the Bragg–Brentano reflection geometry. The general shape of the diffuse scattering was used to investigate defect and amorphous formation during dehydration. The plots of the diffuse scatter are shown in Figure 9. Two distinct diffuse scattering profiles are observed in the data. The first seen in powder patterns from material exposed to very little drying appear as an asymmetric halo peaking at about 40°2θ. The second, seen in powder patterns from material after more extensive drying, exhibits two distinctive well-defined halos at about 19 and 35°2θ, matching the form of the diffuse scattering observed from the amorphous state. The initial diffuse halo increases in intensity and moves to lower angles as the low angle halo splits off with longer drying times. This behavior indicating an increase in the noncrystalline portion of the sample is consistent with the Debye–Einstein formula (Eq. 3) where an increase in the degree of lattice distortion from random defects moves the intensity of the diffuse scattering toward lower angles.

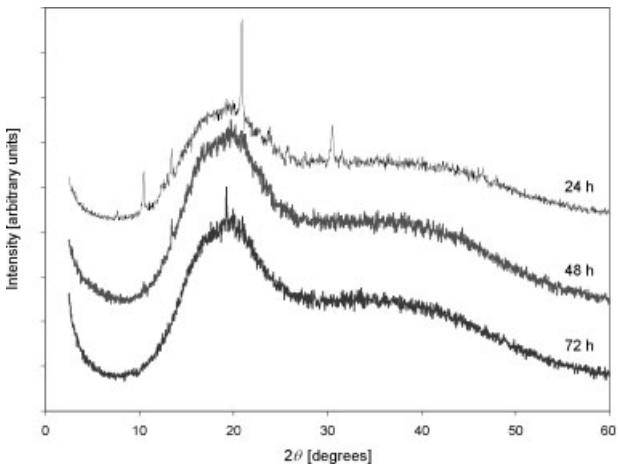

Figure 8. XRPD patterns (reflection) of raffinose pentahydrate after drying at 60°C under vacuum for (from top to bottom): 24, 48, and 72 h.

Using the Rietveld refined crystal structure to derive the continuous Debye structure factor, the Debye–Einstein formula (Eq. 3) was subsequently used to determine the expected diffuse scattering profiles for varying defect strain fields by changing the RMS strain value. The diffuse scattering profiles of the pentahydrate and trihydrate (Fig. 10a and b, respectively) exhibit the general trend of increased scattering at lower angles as the defect strain field increases. The simulated diffuse scattering for the pentahydrate structure agrees very well with the observed diffuse scattering for the 0.5 h drying measurement, as shown in Figure 10c. The diffuse scattering profile observed after the longer drying times of 2 and 5 h is better matched by the diffuse scattering derived from the trihydrate structure, as shown in Figure 10d. However, the double halo shape similar to the X-ray amorphous scattering that appeared for the longer drying time

 DOI 10.1002/jps

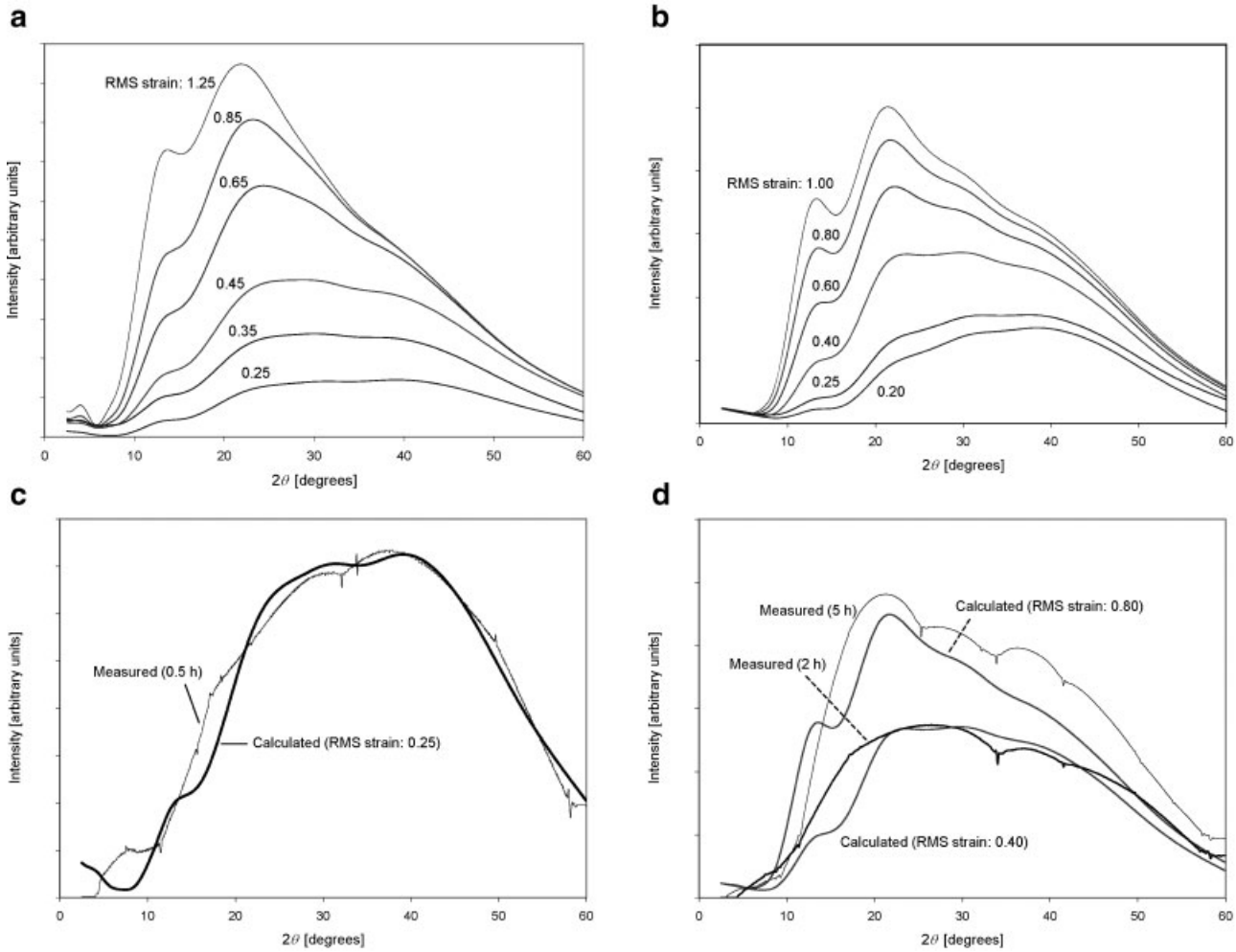

Figure 10. Characterization of diffuse scattering. (a) Debye–Einstein evolution of predicted diffuse scattering for defects in raffinose pentahydrate using RMS strain values ranging from 0.25 to 1.25, (b) Debye–Einstein evolution of predicted diffuse scattering for defects in raffinose trihydrate using RMS strain values ranging from 0.20 to 1.00, (c) calculated diffuse scattering profile for raffinose pentahydrate with respect to the measured diffuse scattering after 0.5 h of drying, and (d) for raffinose trihydrate with respect to the measured diffuse scattering after 2 and 5 h of drying.

measurements of 8 and 24 h could not be accurately described using a continuous structure factor derived form either the pentahydrate or trihydrate crystal structures. The modeling of the X-ray amorphous scattering profile is the subject of ongoing work.

Based on the shape of the diffuse scattering and the results of the random defect modeling, it appears that the diffuse X-ray scattering seen for material dried at 0.5 and 1 h corresponds primarily to increasing defect concentration in the average crystal structure. The diffuse scattering from samples exposed to more extensive drying of more than 5 h closely resembled the X-ray amorphous scattering and could not be modeled in terms of random defects in a raffinose crystal structure. Samples dried for between 1 and 5 h exhibited diffuse scattering best described by a combination of random defects and X-ray amorphous contributions.

The impact of the noncrystalline regions on the raffinose samples (combined defects and amorphous material) can be estimated by comparing the total integrated intensity in the diffuse scattering from defects with the X-ray amorphous contribution and the crystalline contribution. The relative integrated intensity contributions have been extensively used to determine

relative weight percents of different materials present in a single sample. Within this analytical framework while percent crystalline and percent amorphous have some quantitative meaning as two separate phases, percent defects is a more difficult concept as the defects can only exist within the crystalline lattice. Within the scope of this work, the percent defect number is taken to provide a relative indication as to average number of atoms/molecules involved in the defect strain field. Expressing the defect number as number of vacancies is the subject of ongoing work. The total diffuse contribution isolated using the digital filter was modeled with a linear combination of X-ray amorphous and defect components. The ratio was adjusted to give the lowest residual error between the extracted diffuse component and the simulated diffuse component. The final integrated intensity values are summarized in Table 3 and expressed as relative percentages.

The data presented in Table 3 show that increased exposure to the drying conditions increases the total amount of noncrystalline regions present in the raffinose samples. The plot of the percent noncrystalline regions versus time is given in Figure 11. Data for samples dried for 5 h or more exhibit percentage of disordered material formed that are well described by an immediate onset random conversion model and agrees well with data reported previously for dehydrated raffinose pentahydrate.[17] For samples dried less than 5 h, the inclusion of defect scattering into the diffuse profile gives intensity ratios significantly higher than those reported previously and significantly higher than those predicted by assuming conversion as shown in Figure 12. The initial rapid defect built above that predicted by the random single defect model may indicate either a cooperative phenomena or a second independent defect generation process independent of the amorphous phase formation. Once the defect level has reached approximately 14% by diffuse scattering, the conversion to amorphous material takes over. The data in Table 3 show the defect level expressed as a percentage relative to the amount of crystalline material building up to a maximum of approximately 20% and then remaining relatively constant until the last measurement showing a well-defined crystalline structure at the 8 h drying point. Once the amorphous material appears after about 1 h of drying, the amorphous percentage continues to increase until the sample is close to being fully amorphous. Removing the diffuse intensity due to defect scattering gives an increasing amorphous percentage with drying that is very well described by the random conversion model (Fig. 12) with a delayed onset of 0.5 h. The delayed onset of the amorphous curve modeled as a random process again suggests that the initial defect build up is required to drive the amorphous formation.

From the analysis presented in this section, it was possible to separate and quantitate the defects and amorphous regions produced upon dehydration using XRPD data. It is apparent that a number of distinct events occur on the dehydration of raffinose pentahydrate associated with the loss of the two moles of water, as observed in previous studies.[17] There is the local defect build up on the initial water loss followed by the delayed amorphous collapse once sufficient defects have been established. The change in the unit cell parameters of the average crystal structure and the associated volume reduction is also a delayed event which apparently does not unfold until the amorphous collapse has been initiated. The modeling performed in this study, therefore, provided more in-depth information than could

Table 3. Diffuse Scattering Data for Dehydration Studies of Raffinose Pentahydrate

Time (h)[a]	Percent Crystalline	Percent Defects and Amorphous	Percent Defects	Percent Defects per Crystalline Region	Percent Amorphous
0.5	86	14	14	14	—
1	83	17	12	13	5
2	76	24	12	16	12
5	58	42	12	19	30
8	39	61	10	22	51
24	—	89	—	—	89

[a]Hours in 60°C vacuum oven.

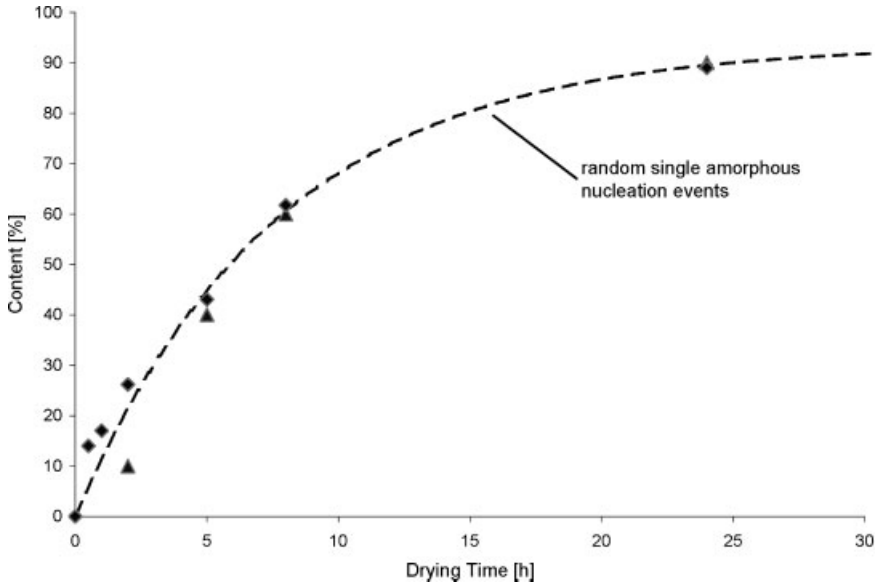

Figure 11. Content of noncrystalline material as a function of drying time for raffinose pentahydrate determined from diffuse scattering data (◆) and XRPD measurements from reference 17 (▲).The theoretical curve is based upon random noninteracting conversion of crystalline to amorphous.

be obtained from conventional methods of assessing percent amorphous by techniques such as moisture sorption,[44] XRPD,[45] and Raman spectroscopy.[46]

CONCLUSIONS

The fact that processing crystalline solids by mechanical means can cause defects in the

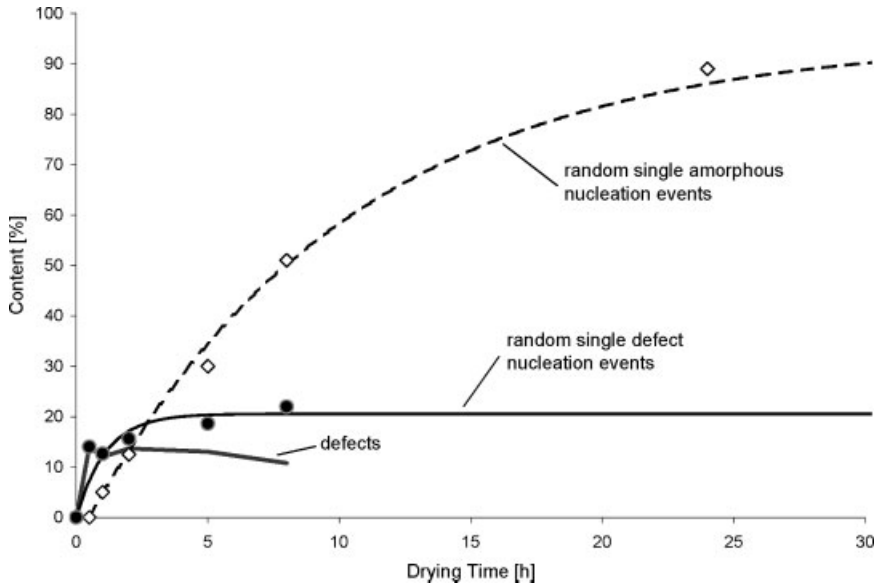

Figure 12. Content of noncrystalline material as a function of drying time for raffinose pentahydrate determined from diffuse scattering data (◇). The percentage amorphous (from Table 3) is denoted with circle markers (●). The theoretical curves are based upon random noninteracting conversion of crystalline to amorphous where (thin line) includes the defect contribution with immediate onset and (dashed line) includes a delayed onset and slower conversion rate for amorphous alone.

crystal followed by a conversion of the crystal to its amorphous form is well established and of significant importance in explaining the enhanced physical and chemical instabilities introduced by pharmaceutical processes such as milling and compaction of APIs and excipients. One of the possible mechanisms by which mechanical stress causes amorphization to occur is the introduction of defects that provide a higher energy and a thermodynamic driving force[14] for further disorder of the crystal. What the present study has shown quantitatively for the first time is that the dehydration of an organic crystal hydrate, such as raffinose pentahydrate, shown previously to become amorphous upon an extended period of heating, well below any melting transition, appears also to be initiated by the formation of defects during the removal of the first two water molecules making up the pentahydrate crystal structure, while retaining the pentahydrate crystal structure. We would suggest that removal of the first water molecules from the pentahydrate creates vacancies, and perhaps other types of crystal defects, that provide the higher energy for subsequent amorphization of the crystals. Therefore, it would appear that a critical factor in whether or not dehydration of a crystal hydrate eventually will cause collapse of the crystal structure to the amorphous form, and how easily this might occur, will depend on the location of the water molecules, the strength of hydrogen bonding with the polar groups of the other molecule, and the extent to which defects are introduced. For example, water located in large "tunnels" within the crystal lattice may have less tendency to produce defects upon removal, leaving the crystal structure intact as a crystal dehydrate. It would be interesting in this regard to carry out such an analysis of defect formation during dehydration with other crystalline hydrates that are known to form amorphous structures upon dehydration, e.g., trehalose dehydrate.[21–23] It should also be mentioned that such a means of amorphization is not limited to the dehydration of crystal hydrates. It has been shown, for example, that the 1:1 acetonitrile crystal solvate of quinapril HCl easily forms amorphous structure upon removal of the acetonitrile molecule by gentle heating.[47] The method developed from the current study can also be used to determine if the removal of the large acetonitrile molecule would initially cause amorphization through a defect-forming mechanism. It can also be used to determine the effects of other processing, such as grinding, on pharmaceutical materials.

REFERENCES

1. Byrn SR, Pfeiffer RR, Stowell JG. 1999. Solid-state chemistry of drugs, 2nd edition. West Lafayette, IN: SSCI, Inc.
2. Cowley JM. 1990. Diffraction Physics, 2nd edition 4th printing. Amsterdam: North-Holland.
3. Zhang J, Ebbens S, Chen X, Jin Z, Luk S, Madden C, Patel N, Roberts C. 2006. Determination of surface free energy of crystalline and amorphous lactose by atomic force microscopy adhesion measurement. Pharm Res 23:401.
4. Burt HM, Mitchell AG. 1981. Crystal defects and dissolution. Intl J Pharm 9:137–152.
5. Huttenrauch R, Fricke S, Zielke P. 1985. Mechanical activation of pharmaceutical systems. Pharm Res 2:302–306.
6. Shalaev E, Shalaeva M, Zografi G. 2002. The effect of disorder on the chemical reactivity of an organic solid, tetraglycine methyl ester: Change of the reaction mechanism. J Pharm Sci 91:584–593.
7. Hiestand E, Smith DP. 1984. Indices of tablet performance. Powder Tech 38:145–159.
8. Wildfong PLD, Hancock BC, Moore MD, Morris KR. 2006. Towards an understanding of the structurally based potential for mechanically activated disordering of small molecule organic crystals. J Pharm Sci 95:2645–2656.
9. Huttenrauch R, Keiner I. 1977. Rekristallisation aktivierter festtstoffe beim verpressen. Die Pharmazie 32:129–130.
10. Huttenrauch R. 1977. Abhangigkeit der hygroscopizitat von der kristallinitat. Die Pharmazie 32: 240–244.
11. Ahlneck C, Zografi G. 1990. The molecular basis of moisture effects on the physical and chemical stability of drugs in the solid state. Int J Pharm 62:87–95.
12. Hancock B, Zografi G. 1997. Characteristics and significance of the amorphous state in pharmaceutical systems. J Pharm Sci 86:1–12.
13. Stillinger FH, Weber TA. 1984. Packing structures and transitions in liquids and solids. Science 225: 983–989.
14. Fecht HJ. 1992. Defect-induced melting and solid-state amorphization. Nature 356:133–135.
15. Berman HM. 1970. The crystal structure of a trisaccharide, raffinose pentahydrate. Acta Crystallogr B 26:290–299.
16. Jeffrey GA, Huang D. 1990. The hydrogen bonding in the crystal structure of raffinose pentahydrate. Carbohydr Res 206:173–182.

17. Saleki-Gerhardt A, Stowell JG, Byrn SR, Zografi G. 1995. Hydration and dehydration of crystalline and amorphous forms of raffinose. J Pharm Sci 84:318–323.
18. Kajiwara K, Franks F. 1997. Crystalline and amorphous phases in the binary system water-raffinose. J Chem Soc Faraday Trans 93:1779–1783.
19. Kajiwars K, Franks F, Echlin P, Greer AL. 1999. Structural and dynamic properties of crystalline and amorphous phases in raffinose-water mixtures. Pharm Res 16:1441–1448.
20. Moura-Ramos JJ, Pinto SS, Diogo HP. 2005. Molecular mobility in raffinose in the crystalline pentahydrate form and in the amorphous anhydrous form. Pharm Res 22:1142–1148.
21. Taylor LS, York P. 1998. Effect of particle size and temperature on the dehydration kinetics of trehalose dihydrate. Int J Pharm 167:215–221.
22. Willart JF, De Gusseme A, Hemon S, Descamp M, Leveiller F, Rameau A. 2002. Vitrification and polymorphism of trehalose induced by dehydration of trehalose dehydrate. J Phys Chem B 106:3365–3370.
23. Ding S-P, Fan J, Green JL, Lu Q, Sanchez E, Angell CA. 1996. Vitrification of trehalose by water loss from its crystalline dehydrate. J Therm Anal 47: 1391–1405.
24. Wellberry TR, Butler BD. 1994. Interpretation of diffuse X-ray scattering via models of disorder. J Appl Crystallogr 27:205–231.
25. Keen DA, Dove MT. 2000. Total scattering studies of silica polymorphs: Similarities in glass and disordered crystalline local structures. Miner Mag 64:447–455.
26. Ferrari M, Lutterotti L. 1994. Method for the simultaneous determination of anisotropic residual stresses and texture by X-ray diffraction. J Appl Phys 76:7246–7255.
27. Matthies S, Lutterotti L, Wenk H-R. 1997. Advances in texture analysis from diffraction spectra. J Appl Cryst 30:31–42.
28. Bates S, Zografi G, Engers D, Morris K, Crowley K, Newman A. 2006. An analysis of X-ray amorphous pharmaceutical solids. Pharm Res 23:2333–2349.
29. Lutterotti L, Matthies S, Wenk H-R. 1999. MAUD (Material Analysis Using Diffraction): A user friendly {Java} program for {Rietveld} texture analysis and more. Proceeding of the Twelfth International Conference on Textures of Materials (ICOTOM-12). 1:1599–1604.
30. Cambridge Crystallographic Data Center. 2006. Version 5.27.
31. Billinge SJL, Thorpe MF. 1998. Local Structure from Diffraction. New York: Plenum Press.
32. Debye P. 1915. Ann d Physik 46:809–823.
33. Proffen T. 2000. Analysis of occupational and displacive disorder using atomic pair distribution function: A systematic investigation. Z Kristallogr 215:1–8.
34. Proffen T, Billinge SJL, Egami T, Louca D. 2003. Structural analysis of complex materials using the atomic pair distribution function—A practical guide. Z Kristallogr 218:132–143.
35. Bishop M, Bruin C. 1984. The pair correlation function: A probe of molecular order. Am J Phys 52:1106–1108.
36. Guinier A. 1994. X-ray Diffraction In Crystals, Imperfect Crystals, and Amorphous Bodies. New York: Dover Publications.
37. Klug HP, Alexander LE. 1974. X-ray Diffraction Procedures for Polycrystalline and Amorphous Material. New York: John Wiley & Sons.
38. Warren BE. 1990. X-ray Diffraction. New York: Dover Publications.
39. Toby BH, Egami T. 1992. Accuracy of pair distribution function analysis applied to crystalline and non-crystalline materials. Acta Cryst A48:336–346.
40. Peterson PF, Bozin ES, Proffen T, Billinge SJL. 2003. Improved measures of quality for the atomic pair distribution function. J Appl Cryst 36:53–64.
41. Petkov V, Billinge SJL, Shastri SD, Himmel B. 2001. High-resolution atomic distribution functions of disordered materials by high-energy X-ray diffraction. J Non-Cryst Solids 293-295:726–730.
42. Peterson PF, Bozin ES, Proffen T, Billinge SJL. 2003. Improved measures of quality for the atomic pair distribution function. J Appl Cryst 36:53–64.
43. James RW. 1962. The optical principles of the diffraction of X-rays. Woodbridge, CT: Ox Bow Press.
44. Saleki-Gerhardt A, Zografi G. 1994. Assessment of disorder in crystalline solids. Int J Pharm 101:237–247.
45. Black DB, Lovering EG. 1977. Estimation of the degree of crystallinity in digoxin by X-ray and infrared methods. Pharm Pharmacol 29:684–687.
46. Taylor LS, Zografi G. 1998. The quantitative analysis of crystallinity using FT-Raman spectroscopy. Pharm Res 15:755–761.
47. Guo Y, Byrn SR, Zografi G. 2000. Physical characteristics and chemical degradation of amorphous quinapril hydrochloride. J Pharm Sci 89:128–143.